

ABSTRACT

STUDIES OF VECTOR BOSON SCATTERING IN THE SEMILEPTONIC ZV CHANNEL WITH THE CMS DETECTOR AT $\sqrt{s} = 13$ TEV

Ramanpreet Singh, Ph.D.

Department of Physics
Northern Illinois University, 2021
Vishnu Zutshi, Director

About Vector boson scattering (VBS)

NORTHERN ILLINOIS UNIVERSITY
DE KALB, ILLINOIS

SEPTEMBER 2021

**STUDIES OF VECTOR BOSON SCATTERING IN THE SEMILEPTONIC
ZV CHANNEL WITH THE CMS DETECTOR AT $\sqrt{s} = 13$ TEV**

BY

RAMANPREET SINGH
© 2021 Ramanpreet Singh

A DISSERTATION SUBMITTED TO THE GRADUATE SCHOOL
IN PARTIAL FULFILLMENT OF THE REQUIREMENTS
FOR THE DEGREE
DOCTOR OF PHILOSOPHY

DEPARTMENT OF PHYSICS

Dissertation Director:
Vishnu Zutshi

ACKNOWLEDGEMENTS

Acknowledge people here.

DEDICATION

To my family.

TABLE OF CONTENTS

	Page
LIST OF TABLES	vi
LIST OF FIGURES	vii
LIST OF APPENDICES	viii
Chapter	
1 INTRODUCTION	1
2 THE STANDARD MODEL	2
2.1 Standard model	2
2.1.1 Fundamental Particles	2
2.1.1.1 Fermions	2
3 THE LHC AND CMS EXPERIMENT	3
3.1 The Large Hadron Collider	3
3.1.1 Integrated Luminosity	5
3.2 The CMS Detector	6
3.2.1 The CMS Coordinate System	8
3.2.2 The Superconducting Magnet	9
3.2.3 The Tracking System	10
3.2.4 The Electromagnetic Calorimeter	11
3.2.5 The Hadronic Calorimeter	13
3.2.6 Muon System	14
3.2.7 Level 1 Trigger	14

Chapter	Page
3.3 High Granularity Calorimeter Upgrade	14
4 EVENT SIMULATION AND RECONSTRUCTION	16
4.1 Object Reconstruction	16
4.1.1 Muons	16
4.1.2 Electrons and Photons	16
4.1.3 Jets	16
4.2 Monte Carlo Simulation	16
4.2.1 Generators	16
4.2.2 Hadronization	16
5 VBS MEASUREMENT IN $ZVJJ$ FINAL STATE	17
5.1 Dataset and Simulation	18
5.1.1 Data	18
5.1.2 MC Simulations	18
5.2 Event Selection	18
5.2.1 HLT Trigger	18
5.2.2 Lepton Selection	18
5.2.2.1 Muon	18
5.2.2.2 Electron	18
5.2.3 VBS Tagged Jets	18
5.2.4 V Jet Candidate	18
6 RESULTS	19
REFERENCES	20
APPENDICES	22

LIST OF TABLES

Table	Page
3.1 Standard physics luminosity for run-2	5

LIST OF FIGURES

Figure		Page
3.1	A schematic of the CERN accelerator complex.	4
3.2	Cumulative delivered and recorded luminosity versus time for 2015–2018 proton-proton collisions	5
3.3	The CMS detector cutaway view	6
3.4	The CMS detector slice view	7
3.5	The picture of the CMS detector central part when lowered in underground cavern with superconducting magnet and iron yoke visible	9
3.6	The CMS pixel upgrade	11
3.7	The CMS ECAL schematic layout	12
3.8	The ECAL endcap quadrant assembled view	12
3.9	The first half of the barrel HCAL inserted into the superconducting solenoid (April 2006)	13
3.10	The HCAL depth segmentation after phase 1 upgrade	14
3.11	The quadrant view of CMS subdetectors layout, and the coverage of the muon detector DTs, CSCs, and RPCs highlighted	15

LIST OF APPENDICES

Appendix	Page
A MACHINE LEARNING	22
B DATA ANALYSIS	24

CHAPTER 1

INTRODUCTION

CHAPTER 2

THE STANDARD MODEL

Introduction to Standard Model (SM), Effective Field Theory (EFT), Vector boson scattering (VBS), etc.

2.1 Standard model

Introduction to SM [1] goes here.

2.1.1 Fundamental Particles

About fundamental particles

2.1.1.1 Fermions

About fermions

CHAPTER 3

THE LHC AND CMS EXPERIMENT

The physics analysis is carried out using Compact Muon Solenoid (CMS) experiment at European Council for Nuclear Research (CERN) Large Hadron Collider (LHC) accelerator. This chapter provides overview of LHC and detail of CMS experiment and its sub-detectors for particle tracking and calorimetry.

3.1 The Large Hadron Collider

The LHC is the largest accelerator located at CERN in Geneva, Switzerland. The main LHC ring is 27 km in circumference and around 50 to 175 m underground. The LHC is built to collide protons at 14 TeV center-of-mass energy, LHC delivered proton-proton collisions at 7 and 8 TeV during run-1 (2010–2012), and at 13 TeV center-of-mass energy during run-2 (2015–2018) [2].

The Figure 3.1 describes CERN accelerator complex. The protons are sourced by ionizing hydrogen atoms and then fed into linear accelerator (LINAC). The LINAC accelerates the protons to 50 MeV and sent to the booster. Then the booster increases energy of protons to 1.4 MeV and feeds it to the proton syncrotron (PS) which further increases energy to 25 MeV and starts bunching them together with bunches 25 ns apart. Then the proton bunches are passed through super proton synchrotron (SPS) which increases energy to 450 MeV and finally sent to main LHC clockwise and counterclockwise rings where they are accelerated to

final energy required which is 6.5 TeV for both bunches going clockwise and counterclockwise to obtain collisions at 13 TeV center-of-mass energy.

The proton-proton collisions occurs at four different location where two general purpose detectors CMS and A Toroidal LHC Apparatus (ATLAS), and two specific purpose detector A Large Ion Collider Experiment (ALICE) and LHC-beauty (LHCb) are located.

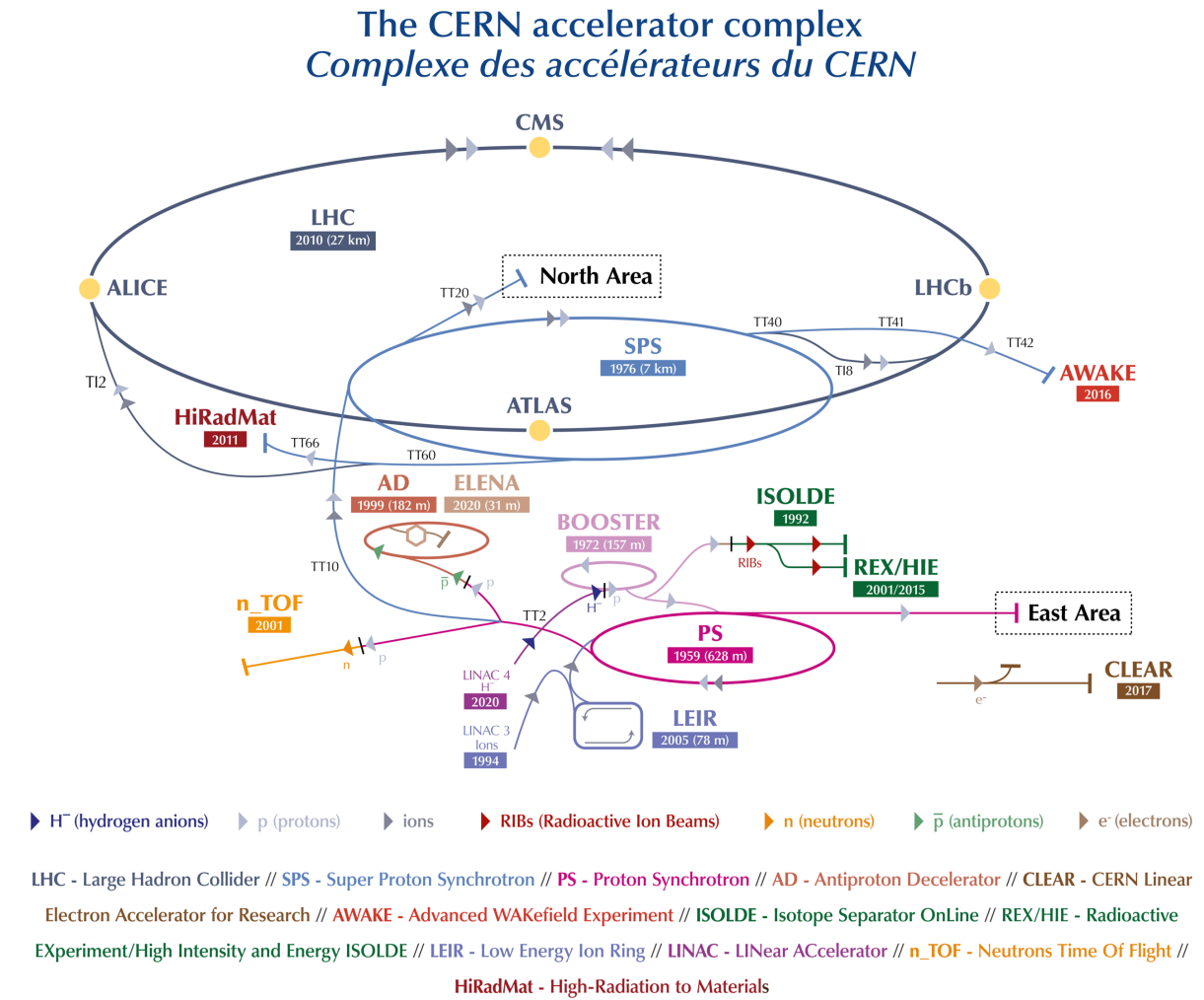


Figure 3.1: A schematic of the CERN accelerator complex [3]

3.1.1 Integrated Luminosity

The number of events generated in a collisions for a given process is

$$N = L\sigma \quad (3.1)$$

where σ is cross-section of the process and L is the luminosity of the LHC.

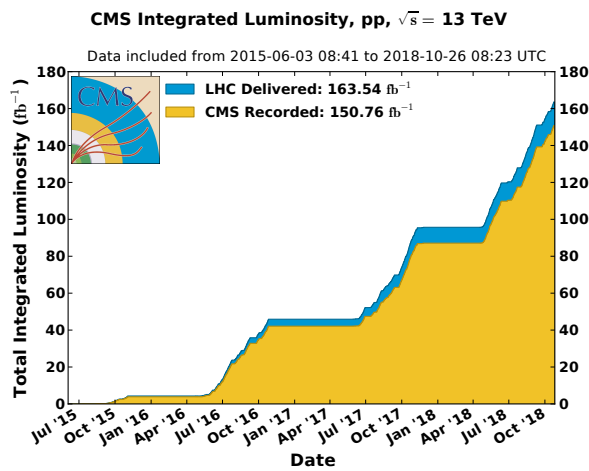


Figure 3.2: Cumulative delivered and recorded luminosity versus time for 2015–2018 proton-proton collisions [4]

Cumulative luminosity delivered and recorded by CMS during run-2 operation is shown in Figure 3.2. For run-2 standard physics analysis luminosity recorded during 2016–2018 is considered, and only runs certified as “golden” by CMS Luminosity physics object group (POG) for analysis are used. The total luminosity for run-2 standard physics is 137.19 fb^{-1} and separately for years in Table 3.1 [5–7].

Table 3.1: Standard physics luminosity for run-2

2016	2017	2018	run-2
35.92 fb^{-1}	41.53 fb^{-1}	59.74 fb^{-1}	137.19 fb^{-1}

3.2 The CMS Detector

The CMS detector is a general purpose detector. A cutaway view of the detector is shown in Figure 3.3. The detector is cylindrical with dimensions 21 meters long, and 15 meters in diameter, and the whole detector weighs about 14000 tonnes. The detector is built in slices with central region called “barrel”, and two closing end sides called “endcap”. A superconducting solenoid generates magnetic field of 3.8 T inside and 2 T outside, and to contain the magnetic field outside of solenoid and support structure of the detector massive steel yokes are used.

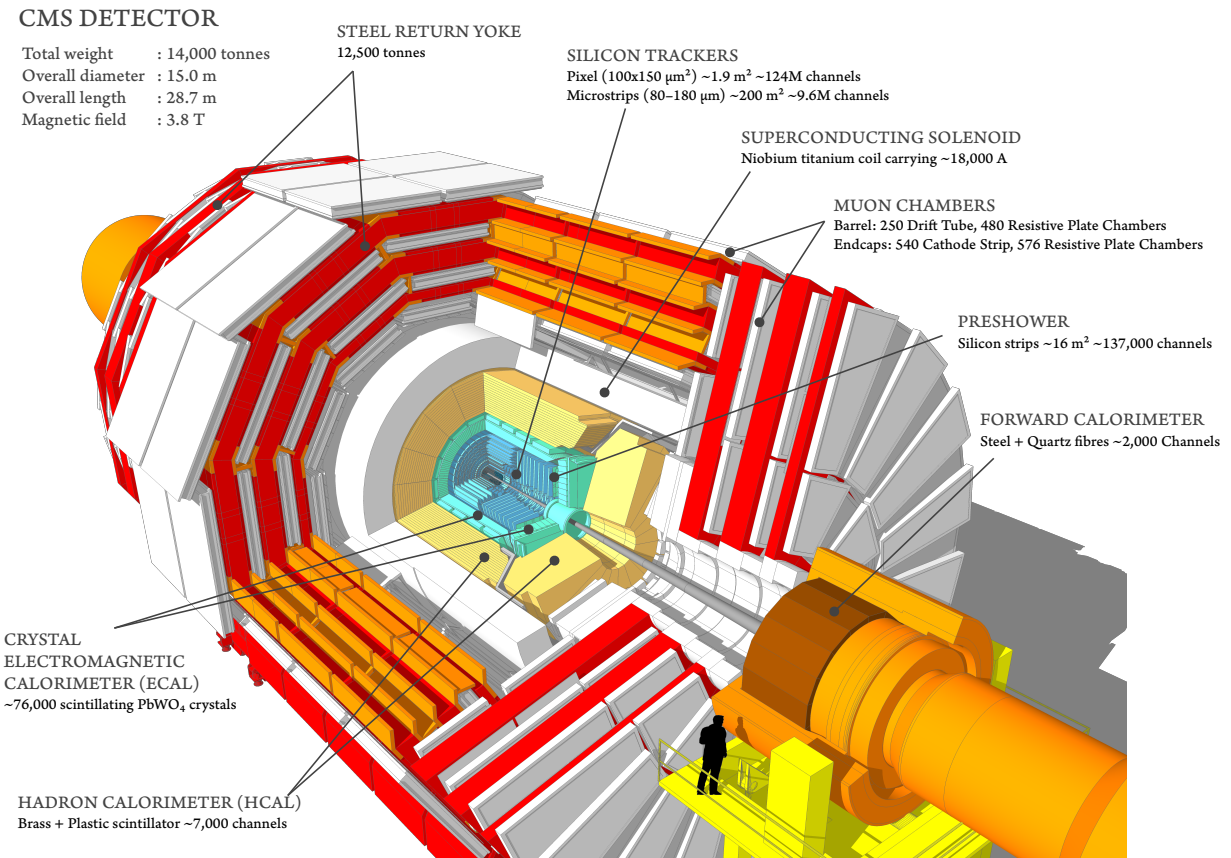


Figure 3.3: The CMS detector cutaway view [8]

The slice view of CMS in Figure 3.4 shows how different particles leave signature in CMS detector. Neutral particles such photons, neutrinos, and hadrons will leave no track in Silicon Tracker (ST), and are identified by only energy deposited or missing energy. Electrons are identified from the track in ST and energy deposit in Electromagnetic Calorimeter (ECAL), hadrons are heavier and they pass through ECAL and deposit their energy completely in Hadronic Calorimeter (HCAL), leaving only small fraction of energy in ECAL. Since muons are minimum ionizing particle (MIP), they pass through whole detector with very small fraction of energy deposit in ECAL and HCAL.

This section describes the subsystems of CMS detector. For detailed technical description refer to [9].

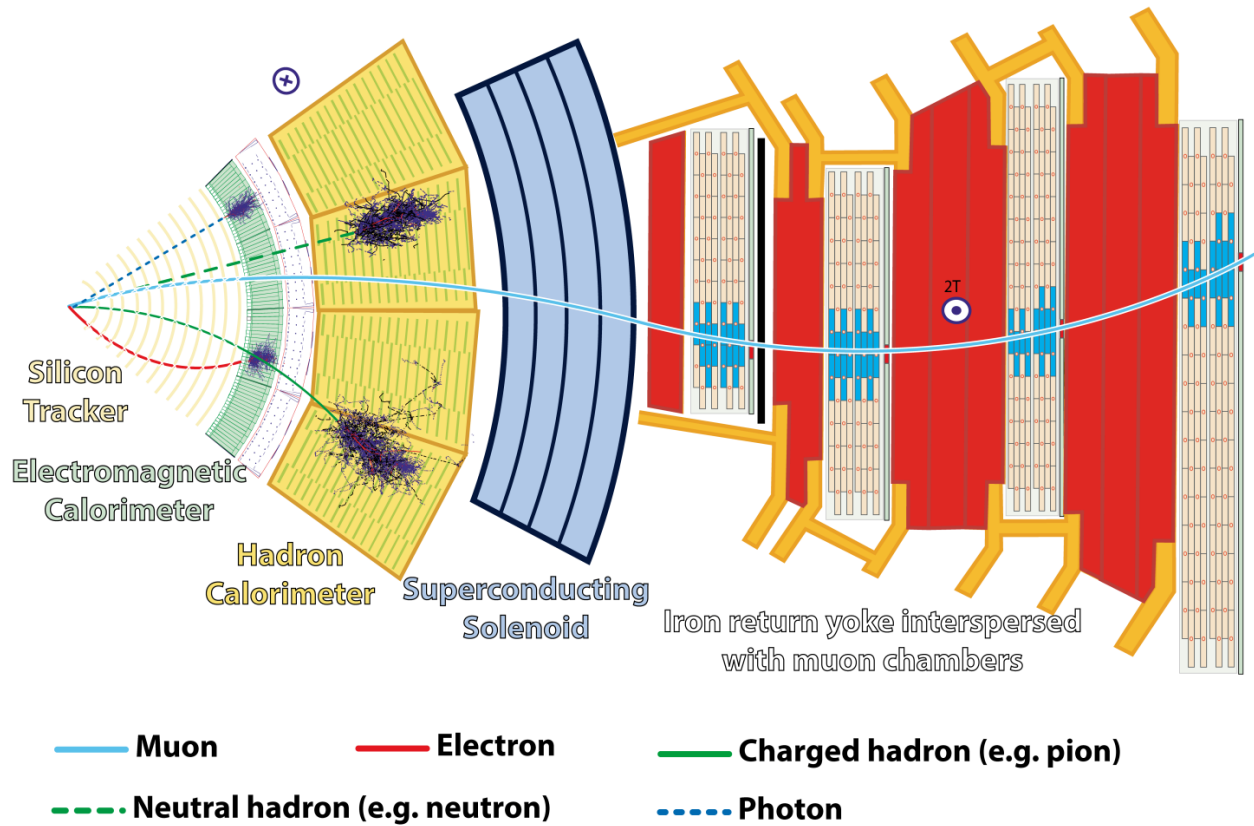


Figure 3.4: The CMS detector slice view [10]

3.2.1 The CMS Coordinate System

CMS uses interaction point (IP) of collisions as origin to define right-handed coordinate system. The z -axis is along the beamline, the x -axis points toward the center of the LHC, and the y -axis points upwards, toward Earth's surface. The transverse plane $x - y$ is used as to calculate most commonly used quantities like transverse momentum p_T and energy E_T .

To describe the direction of particles leaving the IP, azimuthal ϕ and polar θ angles are used. ϕ is measured around the beam axis, and θ is measured from the beam axis. In collider physics, pseudorapidity η (Lorentz invariant) is used to describe direction from beam pipe instead of θ as,

$$\eta = -\ln[\tan \theta/2] \quad (3.2)$$

and sometimes in terms of rapidity y as,

$$y = \frac{1}{2} \ln \frac{E + p_z}{E - p_z} \quad (3.3)$$

Particles kinematics can be completely described in terms of p_T , η , ϕ , and E_T or mass. The distance between the two particles ΔR in $\eta - \phi$ plane is described as,

$$\Delta R = \sqrt{(\Delta\eta)^2 + (\Delta\phi)^2} \quad (3.4)$$

3.2.2 The Superconducting Magnet

The superconducting magnet is the main part of the CMS detector, it is 12.5 meters long and 6.3 meters in diameter. The magnet is cooled to 4.5 K and 20 kA current flows through it to generate 3.8 T of magnetic field with stored energy of 2.6 GJ.

The Figure 3.5 shows visible superconducting magnet and iron yoke when part of CMS detector was lowered in the underground cavern during installation in 2007.

The key purpose of magnet is to determine the momentum and the sign of charged particles by bending them. The momentum resolution of the particles will decrease with increase in p_T , with constant 3.8 T magnetic field inside and it has momentum resolution of $\Delta p/p \approx 10\%$, which is enough to determine unambiguously the sign of muons with momentum of $\approx 1 \text{ TeV}/c$.

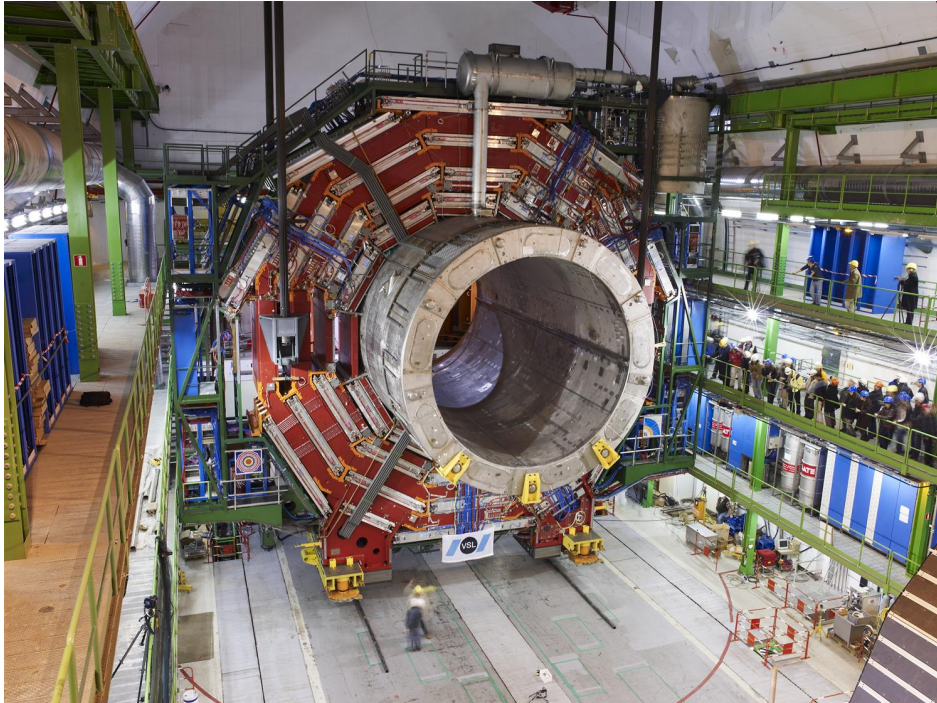


Figure 3.5: The picture of the CMS detector central part when lowered in underground cavern with superconducting magnet and iron yoke visible [11].

3.2.3 The Tracking System

The CMS tracking system ST is the innermost part of the detector, it is made up of pixel and strip detectors. The main goal of ST is to reconstruct the tracks of the charged particles with high precision in high pileup environment.

Silicon is most commonly used material for making tracking systems because of it's semiconductor properties, and high radiation hardness which is essential for the innermost detector. When a p-n junction is built on silicon substrate it creates a depletion zone with no charge carriers at the junction, and whenever a charged particle pass through the depletion zone it creates a electron-hole pair, and under reverse bias this electron-hole generates electrical signal. The CMS tracking consists of about 124 million channels of such junctions in pixel detector and 10 million in strip detector.

The pixel detector was upgraded in 2017 and the comparison of layers before and after the upgrade is shown in Figure 3.6. It is made up of four barrel layers and three endcaps, with nearest barrel layer being 3 cm away from beamline for precise measurement of IP. Because of the large number of pixel channels, the readout is done by Application-specific integrated circuits (ASICs).

The outermost part of ST detector is made of silicon strips. It allows large coverage by reducing number of readout channels. It has 10 layers in barrel region and 12 discs in endcap region. For better signal-to-noise ratio and radiation tolerance both pixel and strip operates at -20 °C.

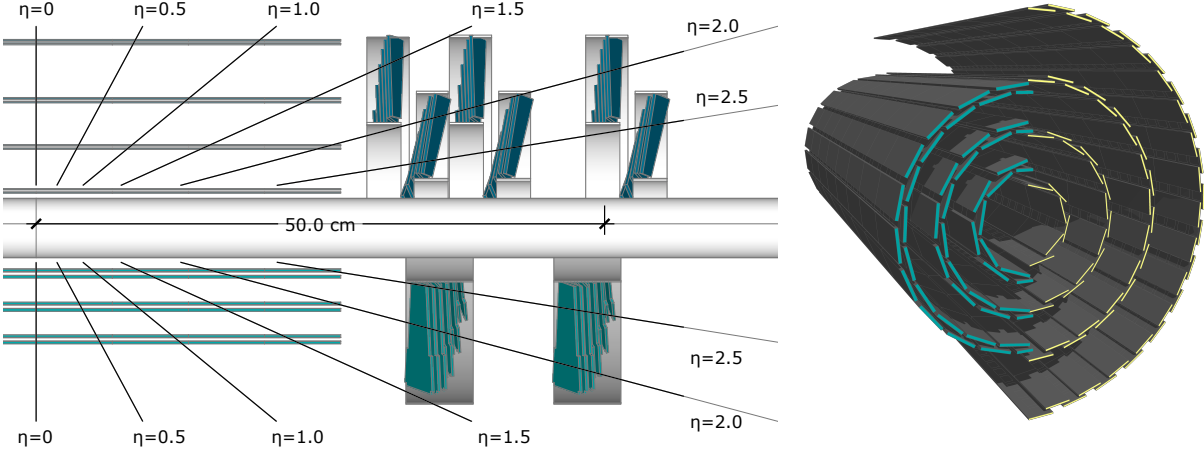


Figure 3.6: The CMS pixel upgrade. The left is cross sectional view of pixel detector layers before upgrade (bottom) and after Phase 1 upgrade (top). The right is view pixel barrel before upgrade (left) and after upgrade (right) [12].

3.2.4 The Electromagnetic Calorimeter

The ECAL active material is made of lead tungstate (PbWO_4) scintillating crystals and two layers silicon strip for preshower in front of the endcaps. The crystals in central barrel section are mounted in quasi-projective geometry pointing towards IP and covers $|\eta| < 1.48$, and two endcaps extends the coverage to $|\eta| = 3.0$. The schematic layout of ECAL is shown in Figure 3.7 and the picture of endcap quadrant when assembled in Figure 3.8

The main purpose of ECAL is to determine energy and positions of electromagnetically interacting particles. To determine particle need to completely deposit their energy, except electron and photons all other particles pass through ECAL crystals with only small fraction of energy signature in crystals. When electron and photon interacts with PbWO_4 it starts the process of electromagnetic shower and continues until the energy the energy of the incident particle is below threshold, which is about 1 MeV.

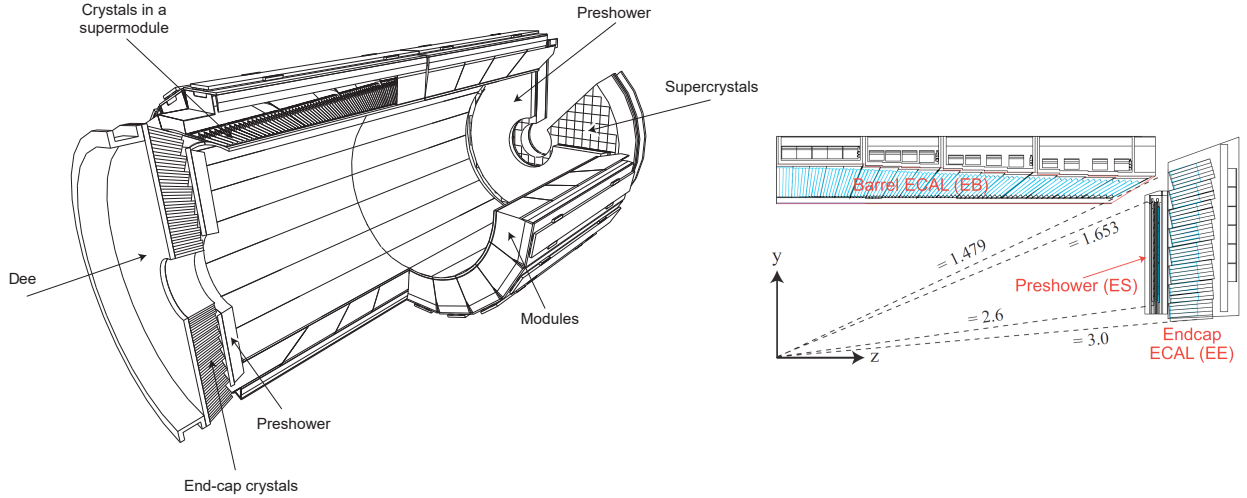


Figure 3.7: The CMS ECAL schematic layout. The left is schematic showing arrangement of superclusters in barrel and endcap (with preshower layers). The right is $y - z$ plane quarter view of ECAL layout [13].

The resolution of the ECAL energy measurements can be described as,

$$\left(\frac{\sigma}{E}\right)^2 = \left(\frac{S}{\sqrt{E}}\right)^2 + \left(\frac{N}{E}\right)^2 + C^2 \quad (3.5)$$

where S is the stochastic term, N is related to the noise, and C is a constant offset.

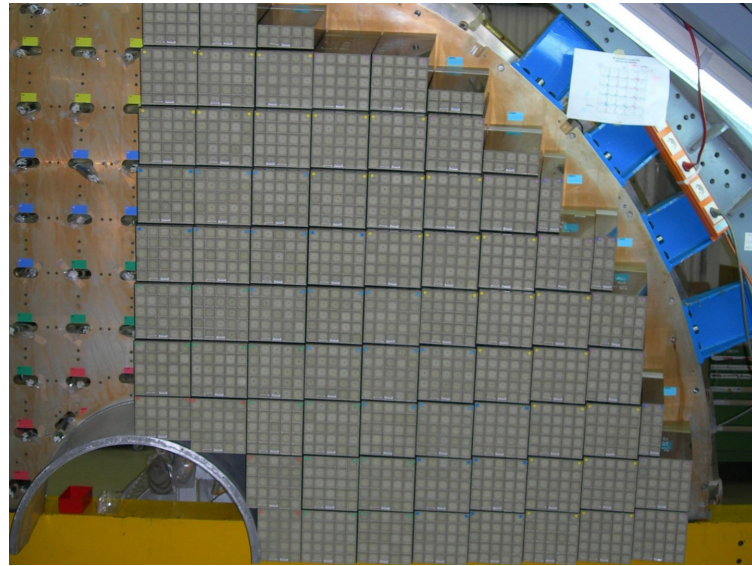


Figure 3.8: The ECAL endcap quadrant assembled view [14].

3.2.5 The Hadronic Calorimeter

HCAL

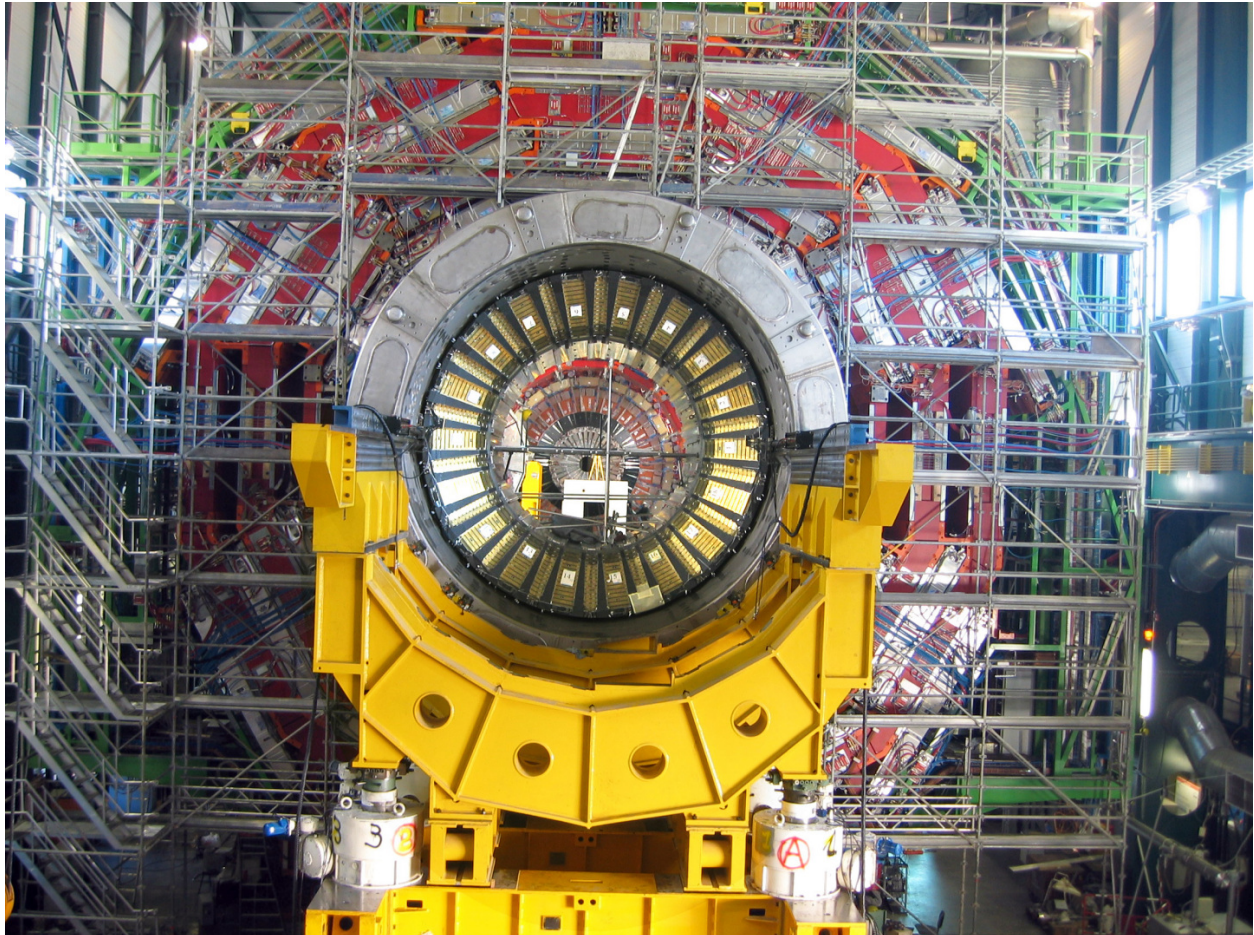


Figure 3.9: The first half of the barrel HCAL inserted into the superconducting solenoid (April 2006) [15].

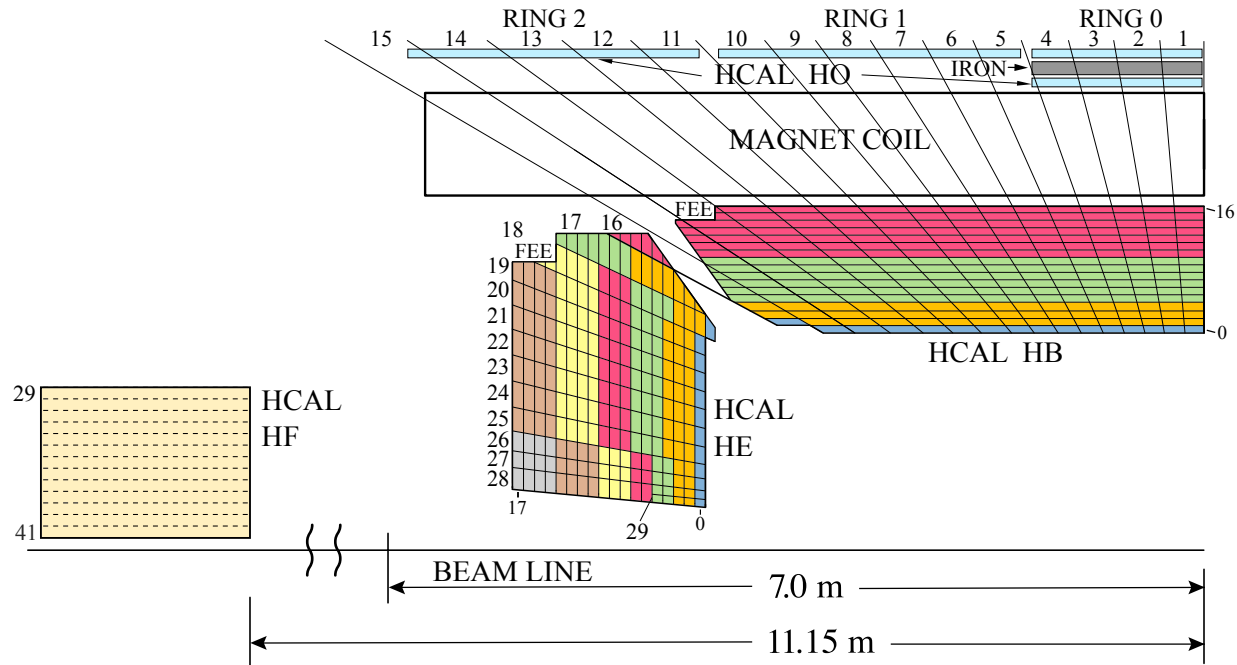


Figure 3.10: The HCAL depth segmentation after phase 1 upgrade [16].

3.2.6 Muon System

3.2.7 Level 1 Trigger

3.3 High Granularity Calorimeter Upgrade

About High Granularity Calorimeter (HGCAL) Upgrade

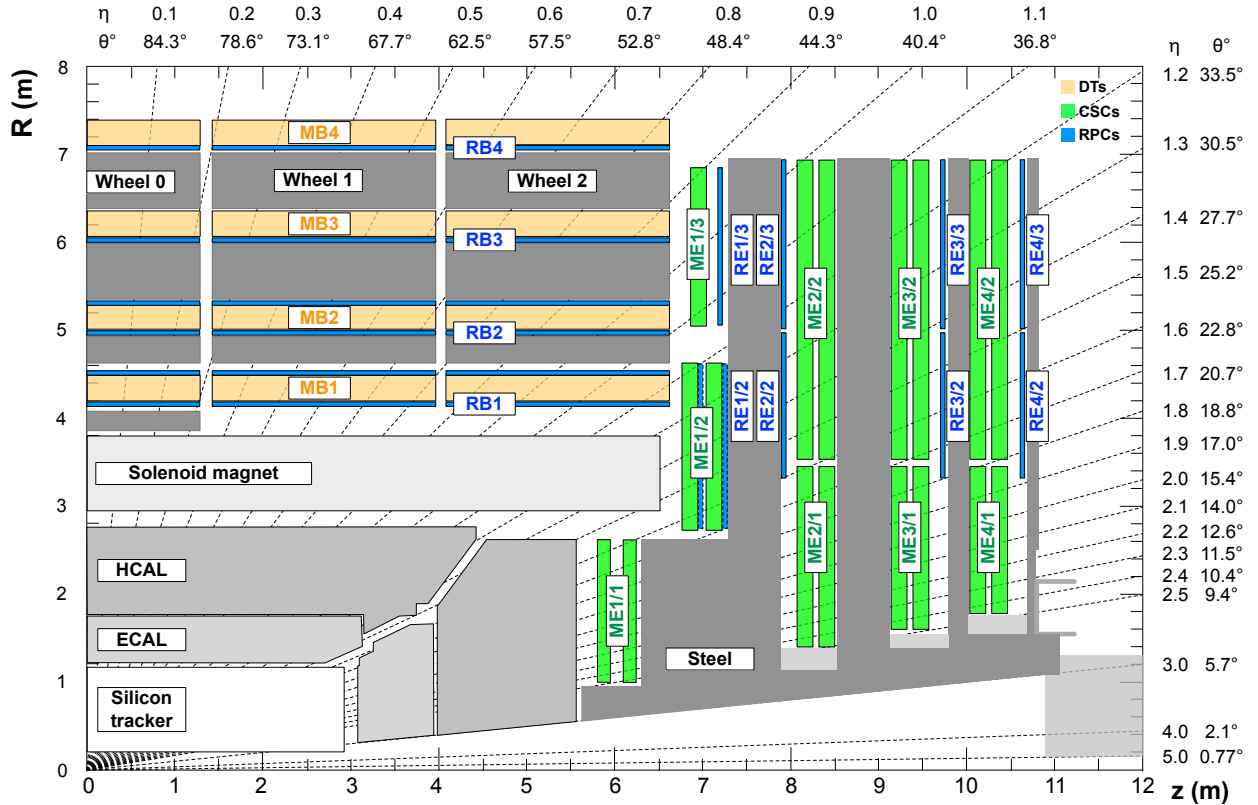


Figure 3.11: The quadrant view of CMS subdetectors layout, and the coverage of the muon detector drift tubes (DTs), cathode strip chambers (CSCs), and resistive plate chambers (RPCs) highlighted [17].

CHAPTER 4

EVENT SIMULATION AND RECONSTRUCTION

4.1 Object Reconstruction

4.1.1 Muons

4.1.2 Electrons and Photons

4.1.3 Jets

4.2 Monte Carlo Simulation

4.2.1 Generators

4.2.2 Hadronization

CHAPTER 5

VBS MEASUREMENT IN $ZVJJ$ FINAL STATE

Analysis of VBS

5.1 Dataset and Simulation

5.1.1 Data

5.1.2 MC Simulations

5.2 Event Selection

5.2.1 HLT Trigger

5.2.2 Lepton Selection

5.2.2.1 Muon

5.2.2.2 Electron

5.2.3 VBS Tagged Jets

5.2.4 V Jet Candidate

CHAPTER 6

RESULTS

REFERENCES

- [1] C. N. Yang and R. L. Mills. “Conservation of Isotopic Spin and Isotopic Gauge Invariance”. *Phys. Rev.* 96 (1 Oct. 1954), pp. 191–195. doi: 10.1103/PhysRev.96.191. URL: <https://link.aps.org/doi/10.1103/PhysRev.96.191>.
- [2] L. Evans and P. Bryant. “LHC Machine”. *Journal of Instrumentation* 3.08 (Aug. 2008), S08001–S08001. doi: 10.1088/1748-0221/3/08/s08001.
- [3] E. Mobs. “The CERN accelerator complex - 2019” (July 2019). Accessed August 16, 2021. URL: <http://cds.cern.ch/record/2684277/files/>.
- [4] Public CMS Luminosity Information. “Cumulative delivered and recorded luminosity versus time for run-2 pp data” (2018). Accessed August 17, 2021. URL: <https://twiki.cern.ch/twiki/bin/view/CMSPublic/LumiPublicResults>.
- [5] The CMS Collaboration. “CMS Luminosity Measurements for the 2016 Data Taking Period” (2017). URL: <https://cds.cern.ch/record/2257069>.
- [6] The CMS Collaboration. “CMS luminosity measurement for the 2017 data-taking period at $\sqrt{s} = 13$ TeV” (2018). URL: <https://cds.cern.ch/record/2621960>.
- [7] The CMS Collaboration. “CMS luminosity measurement for the 2018 data-taking period at $\sqrt{s} = 13$ TeV” (2019). URL: <https://cds.cern.ch/record/2676164>.
- [8] T. Sakuma. “Cutaway diagrams of CMS detector” (May 2019). Accessed August 17, 2021. URL: <https://cds.cern.ch/record/2665537>.
- [9] T. C. Collaboration. “The CMS experiment at the CERN LHC”. *Journal of Instrumentation* 3.08 (Aug. 2008), S08004–S08004. doi: 10.1088/1748-0221/3/08/s08004. URL: <https://doi.org/10.1088/1748-0221/3/08/s08004>.

- [10] The CMS Collaboration. “CMS Detector Slice” (Jan. 2016). Accessed August 18, 2021. URL: <https://cds.cern.ch/record/2120661>.
- [11] M. Brice and C. Marcelloni. “The central part of CMS is lowered” (Feb. 2007). Accessed August 22, 2021. URL: <https://cds.cern.ch/record/1020311>.
- [12] T. Sakuma. “SketchUp Drawings of the Phase 1 pixel detector alongside the current pixel detector” (June 2012). Accessed August 17, 2021. URL: <https://cms-docdb.cern.ch/cgi-bin/PublicDocDB>ShowDocument?docid=6473>.
- [13] The CMS Collaboration. “The CMS ECAL performance with examples”. *Journal of Instrumentation* 9.02 (Feb. 2014), pp. C02008–C02008. DOI: [10.1088/1748-0221/9/02/c02008](https://doi.org/10.1088/1748-0221/9/02/c02008).
- [14] The CMS Collaboration. “Images of CMS ECAL Endcap (EE)” (Nov. 2008). Accessed August 22, 2021. URL: <https://cds.cern.ch/record/1431479>.
- [15] The CMS Collaboration. “Images of the CMS HCAL Barrel (HB)” (2008). Accessed August 22, 2021. URL: <https://cds.cern.ch/record/1431485>.
- [16] The CMS Collaboration. “HCAL Depth Segmentation Phase 1 Upgrade” (2012). Accessed August 22, 2021. URL: <https://home.fnal.gov/~chlebana/CMS/Phase1>.
- [17] The CMS Collaboration. “Performance of the CMS Muon Detectors in early 2016 collision runs” (2016). Accessed August 22, 2021. URL: <https://twiki.cern.ch/twiki/pub/CMSPublic/MuonDPGPublic160729>.

APPENDIX A

MACHINE LEARNING

Write about Machine learning (ML), Multivariate analysis (MVA), Boosted decision tree (BDT), etc.

APPENDIX B

DATA ANALYSIS

Data Analysis Code and Stuff